Konrad-Zuse-Zentrum
für Informationstechnik Berlin

Takustraße 7
D-14195 Berlin-Dahlem
Germany

VINCENT J. DERCKSEN, HANS-CHRISTIAN HEGE,
MARCEL OBERLAENDER

The Filament Editor: An Interactive Software Environment for Visualization, Proof-Editing and Analysis of 3D Neuron Morphology

ZIB-Report 13-75 (November 2013)

Herausgegeben vom
Konrad-Zuse-Zentrum für Informationstechnik Berlin
Takustraße 7
D-14195 Berlin-Dahlem

Telefon: 030-84185-0
Telefax: 030-84185-125

e-mail: bibliothek@zib.de
URL: http://www.zib.de

ZIB-Report (Print) ISSN 1438-0064
ZIB-Report (Internet) ISSN 2192-7782

The Filament Editor: An Interactive Software Environment for Visualization, Proof-Editing and Analysis of 3D Neuron Morphology

Vincent J. Dercksen[*], Hans-Christian Hege[*], Marcel Oberlaender[†‡]

November 28, 2013

Abstract

Neuroanatomical analysis, such as classification of cell types, depends on reliable reconstruction of large numbers of complete 3D dendrite and axon morphologies. At present, the majority of neuron reconstructions are obtained from preparations in a single tissue slice *in vitro*, thus suffering from cut off dendrites and, more dramatically, cut off axons. In general, axons can innervate volumes of several cubic millimeters and may reach path lengths of tens of centimeters. Thus, their complete reconstruction requires *in vivo* labeling, histological sectioning and imaging of large fields of view. Unfortunately, anisotropic background conditions across such large tissue volumes, as well as faintly labeled thin neurites, result in incomplete or erroneous automated tracings and even lead experts to make annotation errors during manual reconstructions. Consequently, tracing reliability renders the major bottleneck for reconstructing complete 3D neuron morphologies. Here, we present a novel set of tools, integrated into a software environment named 'Filament Editor', for creating reliable neuron tracings from sparsely labeled *in vivo* datasets. The Filament Editor allows for simultaneous visualization of complex neuronal tracings and image data in a 3D viewer, proof-editing of neuronal tracings, alignment and interconnection across sections, and morphometric analysis in relation to 3D anatomical reference structures. We illustrate the functionality of the Filament Editor on the example of *in vivo* labeled axons and demonstrate that for the exemplary dataset the final tracing results after proof-editing are independent of the expertise of the human operator.

1 Introduction

During the past 20 years, many technical barriers for reconstructing single neurons have been overcome. Labeling neurons using intracellular (Horikawa and

[*]Department for Visualization and Data Analysis, Zuse Institute Berlin Takustraße 7, 14195 Berlin, Germany. Email: {dercksen,hege}@zib.de

[†]Computational Neuroanatomy Group, Max Planck Institute for Biological Cybernetics. Spemannstraße 38–44, 72076 Tübingen, Germany. Email: marcel.oberlaender@tuebingen.mpg.de

[‡]Department of Digital Neuroanatomy, Max Planck Florida Institute, 5353 Parkside Drive, Jupiter, FL, USA.

Armstrong, 1988) or cell-attached (Pinault, 1996) pipettes has allowed reconstructing large parts of individual neurons (e.g. (Binzegger et al., 2004; Broser, Grinevich, et al., 2008; Broser, Schulte, et al., 2004; Oberlaender, Boudewijns, et al., 2011), thus linking their structure with activity patterns *in vitro* (e.g. (Feldmeyer and Sakmann, 2000; Schubert et al., 2006) and *in vivo* (Oberlaender, Ramirez, et al., 2012). In addition to such conventional techniques, genetic labeling methods based on fluorescent proteins have started the identification and reconstruction of relatively uniform, molecularly identified cell populations (Groh et al., 2010). Further, digital imaging has advanced rapidly. New imaging methods, such as high-speed mosaic/optical-sectioning widefield (Oberlaender, Broser, et al., 2009; Oberlaender, Bruno, et al., 2007) and confocal (Kleinfeld et al., 2011) systems, as well as block-face two-photon (Ragan et al., 2012) and light-sheet (Dodt et al., 2007) microscopes promise high-resolution imaging of large brain regions. Finally, the limitations on archiving terabyte data sets have disappeared with the falling costs of hard disk drives.

As a result of these developments various manual, semi- and fully automated approaches for reconstructing single neuron morphologies have been reported (see (Donohue and Ascoli, 2011; Meijering, 2010) for reviews). The hence rapidly increasing number of reconstructed neuron morphologies gave rise to collaborative efforts that collect single neuron reconstructions – the most comprehensive being the 'NeuroMorpho.org' repository (Ascoli, 2006; Ascoli et al., 2007) – or assemble neuronal network models for computer simulations of cortical signal flow, e.g., the Blue Brain Project (Markram, 2006). However, the vast majority of single neuron tracings has so far been obtained from *in vitro* preparations, i.e., individual neurons are labeled within a tissue slice of usually 300 μm thickness, e.g., the Blue Brain Project relies entirely on *in vitro* tracings (Hill et al., 2012). Unfortunately, *in vitro* tracings suffer from cut off dendrites and axons (Oberlaender, Ramirez, et al., 2012). Reconstructing the complete 3D dendrite and axon morphology of individual neurons, thus requires *in vivo* labeling in combination with histological sectioning of the brain (i.e., due to penetration limits of staining and imaging methods) and subsequent imaging of large tissue volumes. Tracing of faintly labeled, long-range projecting thin neurites, and recovering across-section continuity of neuronal branches, thus render reconstructions of *in vivo* labeled neurons as a major challenge in neuroscience research (e.g., see 'DIADEM' competition (Svoboda, 2011)).

Nevertheless, for sparsely labeled tissue, reconstruction results are usually assumed to be highly reliable. However, little validation of this reliability has been reported (Helmstaedter et al., 2011). Reconstruction validation requires tools that allow users (i) to assess the correctness of the tracings by visual comparison with the image data, and (ii) to interactively correct incomplete or erroneous tracings (Luisi et al., 2011). In addition, in case of *in vivo* data, alignment and interconnection of tracings across brain sections must be established and verified. In consequence, we argue that at present, reconstruction reliability limits the determination of complete 3D morphologies from *in vivo* data.

Here, we present the 'Filament Editor' (FE), an integrated software environment specifically designed to reconstruct and validate single neuron tracings from *in vivo* preparations. It comprises tools for visualizing and interactively correcting 3D neuron tracings, alignment, and across-section continuity, allowing for efficient proof-editing within and across brain sections. In addition, the FE incorporates advanced annotation and morphometric analysis functionali-

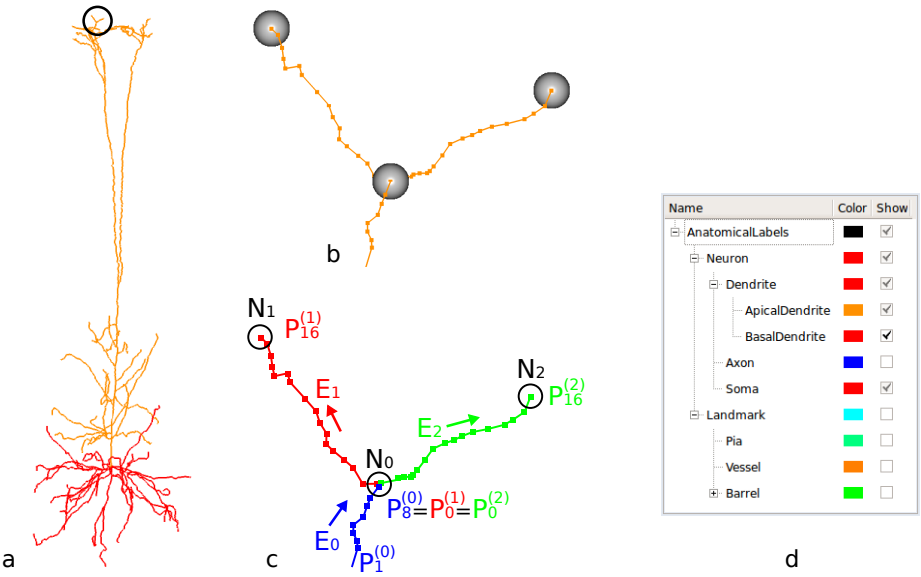

Figure 1: *The SpatialGraph data structure. (a) Dendritic tree of a layer 5 pyramidal neuron (Oberlaender, Kock, et al., 2012), colored according to the anatomical labels defined in (d). (b) Magnification of the encircled region of (a). The nodes (grey spheres) are connected by edges, represented and displayed as polygonal lines defined by edge points (or points, for short; displayed as squares). (c) Schematic representation of the SpatialGraph object in (b). The object consists of three directed edges (E_0, E_1, E_2) which interconnect nodes N_0, N_1, N_2 (the source node of E_0 is not displayed). At branching nodes, the last point of the incoming edge ($P_8^{(0)}$ on edge E_0) coincides with the first point of the outgoing edges ($P_0^{(1)}$ and $P_0^{(2)}$ on E_1 and E_2 respectively). (d) Semantic information can be associated with the morphology using labels. The* Label viewer *is used for editing label hierarchies, assignment of labels to graph elements, and selection of these elements for editing, visualization and analysis.*

ties. We illustrate the applicability of the FE on frequently occurring use cases and demonstrate that the proof-editing routines can result in unambiguous tracings of *in vivo* labeled axons.

2 Methods

2.1 Data structure

The Filament Editor has been developed based on Amira software (FEI-Visualization Sciences Group, 2013a), a visualization framework, implemented in C++, which is frequently used in neuroscience research (e.g. (Ertürk et al., 2012; Halavi et al., 2012), NeuroMorpho.org accepts Amira file format).

Neuron morphology is represented in the FE by the *SpatialGraph* data structure (Fig. 1), which is similar to previously reported graph formats (Mayerich et al., 2011). Specifically, the topological skeleton of the graph is defined by a set of nodes, connected by a set of (unbranched) edges. The edge direction is

defined by specification of the source and target node. Edges can be treated as undirected by ignoring this information. The graph is embedded in space by associating 3D coordinates with each node. The edge trajectory is defined by a sequence of 3D points (vertices). The first and last point of each edge coincides with the source and target node, respectively.

The data structure was designed to allow interactive editing and rendering of large 3D tracings (e.g. >10k edges, >1M points). For traversing the graph, an adjacency list is maintained for each node. This approach is more memory-efficient than adjacency matrices (Skiena, 1998) for storing the present sparse graphs. Further, the explicit representation of the (high-level) topological structure using nodes and edges allows for more efficient traversal than through linked lists of (low-level) points (e.g. SWC (Cannon et al., 1998)) or segments (e.g. *MorphML* (Crook et al., 2007)). Points are stored as coordinate arrays per edge for efficient rendering as line strips.

Different types of attribute data can be associated with the nodes, edges and points of the *SpatialGraph* for visualization and morphometric analysis. Labels are used to associate semantic information with substructures of the graph, e.g. 'Dendrite', 'Axon' and 'Soma' (Fig. 1a,d). Additionally, numerical attributes can be defined, e.g. a floating-point value representing the radius at each edge point. Multiple attributes can be defined on nodes, edges and points simultaneously. For each attribute defined on nodes, an array is generated holding one value for each node. The array size thus equals the number of nodes. Edge and point attributes are stored analogously. The attribute arrays are kept up-to-date throughout the editing process to match the graph structure. Tracings can be imported into the FE using the *SWC* (Cannon et al., 1998), *hoc* (Carnevale and Hines, 2006) or the *amiramesh* (FEI-Visualization Sciences Group, 2013b)) file format. These formats, as well as *MorphML* (Crook et al., 2007) can be used to export the tracings.

2.2 Visualization

The FE provides a 2D and 3D viewer (Online Resource 1) for proof-editing a tracing. The 3D viewer of the FE displays the graph using spheres for the nodes, squares for the points and polylines for the edges. The user can inspect the spatial structure of the tracing in 3D by camera rotation, zooming and panning using the mouse, and edit each of the graphs' components. Nodes, edges and points can be colored according to one of the label attributes. Their displayed size is user-adjustable. Besides traced morphologies, the 3D viewer can display additional data using any available Amira display module (FEI-Visualization Sciences Group, 2013b). For example, the neuron morphology can be jointly visualized with the image data using volume rendering, 2D slices or intensity projections. The *SpatialGraph* can be visualized as tubes by mapping a radius attribute defined on edge points to cylinder thickness (rendering is based on (Sigg et al., 2006)).

The 2D viewer displays a slice of user-defined thickness of the graph, superimposed on a maximum intensity projection (MIP) of the corresponding 3D image region (FEI-Visualization Sciences Group, 2013b). Hiding the remaining image and tracing regions provides an unobstructed view to locally verify the tracing with respect to the image stack. By varying the slice depth and/or orientation, the user navigates through the volume. The slice MIP and bounding

box can be displayed in the 3D viewer to provide additional spatial orientation.

Both viewers can be used either side-by-side or one may be used exclusively. User-selected sets of nodes and edges can temporarily be hidden in both viewers by excluding them from rendering. Images are using standard bitmap formats such as *BMP*, *JPEG*, *PNG*, and *TIFF*, or in the *amiramesh* format. Stacks of 2D images are converted into 3D volumes during import.

2.3 Selection tools

Modification of the traced morphology is achieved by selecting one or more elements (nodes, edges, points), followed by the invocation of an operation (e.g. deletion) (McGuffin and Jurisica, 2009). To provide a selection system that is 'powerful' (i.e. allowing efficient selection of any subset of elements) and 'forgiving' (i.e. the selection itself can easily be modified) (Wills, 1996), the following tools are available in the FE:

- Single-Element Selection: selects single nodes, edges or points that have been clicked on with the mouse.
- Connected-Component Selection: selects the entire subgraph connected to the element that has been clicked on with the mouse;
- Lasso Selection: selects all nodes and edges within a user-drawn polygon. Using a modifier key, only connected components that are completely contained within the Lasso polygon are selected.
- Select-All, Clear and Invert Selection: selects the entire *SpatialGraph*, deselects and inverts the current selection, respectively.
- Label Selection: selects graph elements with a particular attribute by clicking on the respective label in the Label Viewer (Fig. 1d).

Holding a modifier key adds to the current selection. Selected items are highlighted in red in the viewers.

2.4 Editing operations

The following operations are available to manipulate the data structure:

- Deletion of selected nodes and edges;
- Splicing (connecting) edges. Splicing is achieved by selecting either two nodes, two points, or one point and one node, followed by the invocation of the connect operation. Nodes are connected by a new straight edge. Selected points are converted to nodes as they will be branching points; the new nodes are subsequently connected. The splicing operation connects multiple selected elements at once as follows. First, all nodes and edges connected to the currently selected elements are added to the selection, resulting in multiple connected subgraphs. An edge is added between any two terminal nodes from different subgraphs that have the smallest Euclidean distance until all subgraphs are connected.

- Point-to-Node Conversion converts a selected point into a node, resulting in an edge split. The inverse Node-to-Point operation concatenates two edges, while removing the intermediate node. The latter can be run for a single selected node or for all intermediate nodes at once. Together with the Remove-Isolated-Nodes operation, all nodes that are neither branching nor terminal nodes can be purged from the graph.

- Edge-smoothing. Edges are smoothed by repositioning their edge points as follows: the user specifies the neighborhood size N, which must be odd. The position of each point $\mathbf{p}_i$ on the edge is replaced by the average of its own position and the $M = (N-1)/2$ points along both directions:

$$\mathbf{p}_i^{'} = \frac{1}{N} \sum_{k=i-M}^{i+M} \mathbf{p}_k \tag{1}$$

  The first and last M points on the edge are not moved, effectively leaving all nodes in place.

- Transformation. An affine transformation can be applied to tracings, images or any other 3D data set (FEI-Visualization Sciences Group, 2013b). For example, a linear scaling could be applied, independently for all dimensions, to compensate for tissue shrinkage.

All editing operations can be undone/redone. Shortcut keys are defined to efficiently switch between the different selection and editing tools, as an alternative to clicking tool buttons (Nielsen and Mack, 1994).

2.5 Semantic labels

Semantic information can be associated with nodes, edges and points by assigning labels. A label is a name (i.e. a string), uniquely identified by an integer value and associated with a color. Labels are organized in a hierarchical fashion, i.e. in a tree data structure, providing access to graph substructures at different levels of detail. Upon creation of a node (or edge/point) label attribute, each node (or edge/point) is assigned a label from the tree.

The *Label Viewer* (Fig. 1d) is part of the FE user interface allowing the user to (i) define and edit custom label trees, (ii) assign labels to selected substructures of the graph and (iii) select these substructures for editing, visualization and analysis (Online Resource 2). For example, one could define a hierarchical label tree with root label 'Neuron' having child labels 'Axon' and 'Dendrite' and assign these to the respective edges and nodes. Selecting the root label (i.e. 'Neuron') in the Label Viewer highlights all edges and nodes assigned to child labels recursively (i.e. 'Axon' and 'Dendrite'), while selecting 'Dendrite' would highlight the subset of 'Dendrite' elements exclusively. Alternatively, the Label Viewer supports flat label hierarchies (i.e., only one level of labels below the root). For example, the 'identify loops' functionality of the FE (FEI-Visualization Sciences Group, 2013b) automatically assigns all edges comprising a loop the same label, pinpointing potential autapses (i.e., an intersecting dendrite and axon from the same cell) or falsely connected branches.

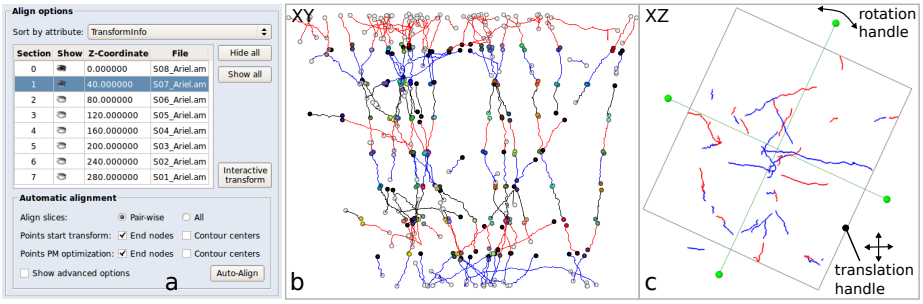

Figure 2: *Section alignment. (a) The* Align *toolbox provides access to both automated and interactive alignment. The section list allows to (i) select a section to align, (ii) toggle section visibility, and (iii) manually adjust the z-position of a section. (b) XY-view after alignment of eight sections. Edges are colored by section, alternating red, blue, and black. Nodes are colored by matching result. Matching nodes in different sections are assigned the same label, and thus the same color. Black nodes could not be matched; white nodes were not used for alignment. (c) Interactive alignment using a handle. Only the section that is currently transformed (red, highlighted in the table in (a)) and its predessor (blue) are visible; other sections are hidden not to obscure the view.*

2.6 Section alignment

The FE incorporates an automated method (Dercksen et al., 2009) for rigid alignment (Zitová and Flusser, 2003) of tracings obtained from adjacent image stacks, e.g. from consecutive brain sections (Online Resource 3). The automated algorithm is complemented with a user interface for interactive manual alignment (Fig.2a).

First, tracings from adjacent image stacks are merged using the *CreateSpatialGraphStack* module. This module generates a new *SpatialGraph* by positioning tracings from image stacks obtained from adjacent brain sections at either fixed distances along the z-axis (i.e. perpendicular to the cutting plane) or such that the bounding boxes adjoin. Tracings from image stacks obtained from the same brain section can be merged without (z-)translation for subsequent manual alignment. The nodes and edges are assigned identifier labels that refer to the corresponding image stack. Transformations can thus be applied to tracings of each individual stack by transforming all nodes and edges with a particular label.

The stack of tracings is aligned by repeated pair-wise alignment of neighboring sections. The automated method (Dercksen et al., 2009) uses a 2D point matching approach to compute the optimal transform, i.e. a rotation angle around the z-axis and a 2D translation parallel to the xy-plane. The points to be matched are the terminal nodes in the top and bottom region of each section, e.g. within the upper and lower 25% (Fig.2b). The algorithm seeks to maximize the number of matching points, while minimizing the positional difference between matched points, weighting these conflicting goals, similar to other feature-based alignment methods (Szeliski, 2006). This approach is sufficiently fast to be used in an interactive workflow (Dercksen et al., 2009), with response times ranging from a fraction of a second for a small number of end

points (∼30), to several seconds for a larger set (∼100).

Sections can be aligned simultaneously or pair-wise. The resultant alignments immediately appear in the 3D viewer, allowing visual validation (Fig. 2c). In cases where the automated alignment result is not satisfactory, the user can interactively translate and rotate each section with respect to its predecessor section in the 3D viewer using handles. All other sections can be hidden to not obscure the view.

2.7 Interactive manual tracing

The interactive tracing functionality available in the 2D viewer (FEI-Visualization Sciences Group, 2013b) can be used to manually add filamentous and/or anatomical reference structures. The user adds new nodes by clicking on the desired location in the image. The node is added at the mouse cursor position at the depth of the image plane (for 2D images) or the depth with highest image intensity (3D image). The node is automatically connected to the latest created node by a new edge. This feature can be used to augment automatically generated tracings, for example with contours representing anatomical landmarks, such as pia, white matter or blood vessel outlines (Fig. 3a), as well as with 2D outlines of the soma in different optical and or histological sections.

2.8 Visual and quantitative morphometric analysis

The FE includes the following functionalities, for visual and quantitative morphometric analysis (Fig. 3):

- Branch length and node statistics (number of branching, terminal nodes) for the entire graph or for a selected subgraph, grouped by semantic labels.
- Quantitative measurement and visualization of branches within/outside a reference volume (Fig. 3a). Closed 3D surfaces representing such reference volumes can be generated from 2D contour outlines of anatomical landmarks, as well as from contours representing neuron somata (Fuchs et al., 1977). The length contained within a volume is computed by intersecting all edge segments with the triangles comprising the bounding surface, performing a point location test (Skiena, 1998) and accumulating the length of the confined branches. The result is output to a spreadsheet. The parts of the morphology contained within a volume can further be visualized by labeling the edge points by the name of the respective structure and coloring the graph according to these labels (Fig. 3a).
- 3D density of morphological properties. A 3D grid of user-defined voxel size is superimposed onto the morphology and morphological properties of the tracing within each voxel (Fig. 3b) are computed. Particular properties of interest are the number of branching nodes or branch length. Branch length within a voxel is computed by clipping each segment between adjacent edge points against the voxel's bounding box (Liang et al., 1992) and accumulating the resulting lengths. Semantic labels allow distinguishing between substructures.
- 1D profile of morphological properties. By accumulating the values in voxels in each plane (e.g. having the same z-value) of the 3D voxel grid

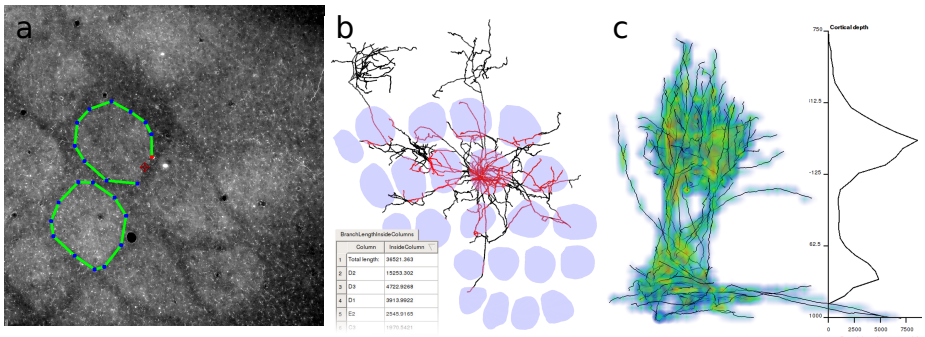

Figure 3: *Morphometric analysis. (a) Manual drawing of anatomical landmark contours. Contours outlining so called 'barrel columns' in rat vibrissal cortex (S1) are created by clicking on the MIP image. A new node (red) is automatically connected to the previously created node by an edge (green). (b) Visual and quantitative analysis of semantically labeled neuronal branches with respect to anatomical reference structures. Here, axonal length of a Layer 5 slender-tufted pyramidal neuron is evaluated with respect to the barrel columns in S1 (Oberlaender, Boudewijns, et al., 2011). The axon length within and outside each column was automatically computed, exported to a spreadsheet, and visualized using the Filament Editor by labeling all edge points as either inside (red) or outside (black) any cortical column. (c) Branch density visualization and quantification. A grid of* $50\,\mu m$ *voxels is superimposed onto a reconstructed thalamocortical axon labeled in rat vibrissal thalamus in vivo (Oberlaender, Ramirez, et al., 2012). For each grid cell the total axon length is computed and visualized in 3D or as 1D density profile by accumulating length densities across each xy-plane.*

described above, a 1D profile of the property of interest along an axis can be extracted (see Fig. 3c and (Meyer et al., 2010; Oberlaender, Kock, et al., 2012)).

2.9 Visual and quantitative comparison of tracings

Quantitative comparison of tracings obtained from the same image data set requires defining their correspondence. Because of the intricate relation between topology and geometry, at present, correspondence definitions need to employ heuristics (Gillette et al., 2011; Mayerich et al., 2011).

Here, we implemented such a comparison metric, based on (Helmstaedter et al., 2011), as follows: Given the set of reconstructions $R_1, \ldots, R_N$ (N being the number of users), first, edge points are inserted on all edges (without modifying the trajectory), such that the distance between any two edge points is smaller than a maximum sampling distance D.

Second, the reconstruction R_1 is pair-wise compared to the reconstructions of all other users $R_2 \ldots R_N$. For each edge point $\mathbf{p}$ on R_1 the number of reconstructions is counted that have a point $\hat{\mathbf{p}}$ that corresponds to $\mathbf{p}$. $\hat{\mathbf{p}}$ corresponds to $\mathbf{p}$ if they are no further than a maximum correspondence distance R apart, i.e., $|\hat{\mathbf{p}} - \mathbf{p}| \leq R$. This results in the number of corresponding edge points $C(\mathbf{p}) \in [1, N]$; $C(\mathbf{p}) = 1$ if there is no other reconstruction with a matching

point (R_1 agrees only with itself in $\mathbf{p}$), $C(\mathbf{p}) = N$ if all other reconstructions have a matching point.

Third, the total length of all edges of R_1 is divided among N bins $L_1, \ldots, L_N$. A bin L_i represents the length of R_1 that was agreed on by i reconstructions. To this end all straight segments between pairs of successive edge points $\mathbf{p}$ and $\mathbf{q}$ are regarded. If $C(\mathbf{p}) = i$, then half the length of segment $\mathbf{pq}$ is added to L_i, same for $\mathbf{q}$. The length bins are computed separately for all other reconstructions $R_2, \ldots, R_N$. The length per bin is presented to the user in a spreadsheet.

To visualize the correspondences, an integer attribute is defined on the edge points, storing the value of $C(\mathbf{p})$ for each point. Displaying one or more reconstructions colored according to this value, similar to (Mayerich et al., 2011), effectively pinpoints inter-user differences.

3 Results

3.1 Application example: 3D reconstruction of individual axons labeled *in vivo*

We illustrate a potential workflow using the tools of the FE to generate complete 3D morphologies for the example of *in vivo* labeled axons, reconstructed by a previously reported automated imaging and tracing pipeline (Oberlaender, Bruno, et al., 2007). The example workflow consists of the following steps: (i) preprocessing: sample preparation, imaging, and tracing, (ii) proof-editing of tracings of individual image stacks and (iii) alignment and proof-editing of tracings across multiple image stacks. The steps will be described in detail below and are illustrated by Online Resources 1-3.

3.1.1 Preprocessing: sample preparation, imaging and tracing

Briefly, individual neurons in rat vibrissal thalamus (for a gallery of reconstructed cells see (Oberlaender, Ramirez, et al., 2012)) were filled with biocytin using whole-cell (Margrie et al., 2002) patch-clamp recordings *in vivo*. This technique allows labeling the complete dendritic and axonal projections of individual neurons (Horikawa and Armstrong, 1988). After perfusion, brains were fixed and cut into 50 μm thick consecutive vibratome sections. Histological staining with DAB (Wong-Riley, 1979) enhances the contrast of the biocytin-labeled neuronal branches in each section. Using a custom-designed mosaic/optical-sectioning brightfield microscope (Oberlaender, Broser, et al., 2009; Oberlaender, Bruno, et al., 2007) and Surveyor image acquisition software (Objective Imaging Ltd.), 3D image stacks of typically $2\,mm \times 2\,mm \times 0.05\,mm$ volumes were acquired in vibrissal cortex at a resolution of $0.184\,\mu m \times 0.184\,\mu m \times 0.5\,\mu m$ per voxel (i.e., at 100× magnification).

Neuronal structures were automatically extracted from eight consecutive image stacks using a previously reported and validated automated tracing software named *NeuroMorph* (Oberlaender, Bruno, et al., 2007). Projection images of each image stack, as well as 3D skeletons of neuronal branches (i.e. *SpatialGraph* files) represent the final results of the automated pipeline for each brain section. A position label is assigned to all edges. The labels indicate whether the connected component containing the edge (i) touches the top of the section

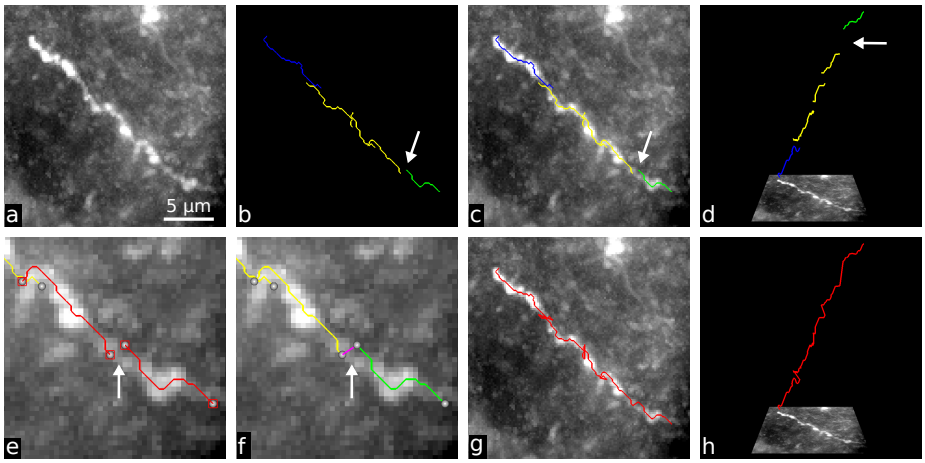

Figure 4: *Splicing fragmented branches. (a) In the 2D MIP image (from an inverted brightfield image stack) an axon fragment can be clearly distinguished from background. (b) Based on 3D information, the automated tracing algorithm generated a fragmented result (possibly due to faintly stained regions in the axial direction), with connected components labeled as touching top (blue), bottom (green) or neither top nor bottom (yellow). (c) MIP and tracings are superimposed in the FE. (d) Rotating the view immediately reveals the order in which the axonal fragments have to be spliced. (e) After zooming in on the region pointed at by the arrow, two branches are selected. (f) The selected branches are connected using the splicing tool, resulting in an added edge segment (magenta). (g) Splicing of the remaining fragments. (h) The 3D view facilitates visual validation.*

(blue), (ii) touches the bottom (green), (iii) passes through (i.e. touches top and bottom; red) or (iv) touches neither top nor bottom (yellow). Thus, a fragmented neuronal process passing through an image stack generally consists of one or more green, zero or more yellow, and one or more blue parts (Fig. 4).

3.1.2 Proof-editing of tracings from individual image stacks

The FE is used to interactively splice (connect) fragmented edges and to delete falsely traced edges from the automated tracing in each individual section. The user loads the automatically traced neuron fragments and displays them in the 3D viewer, colored by position labels. The tracing data is superimposed on the maximum intensity projection image (MIP) of the respective image stack. Four typical proof-editing situations are illustrated in Figures 4–7.

Case 1: *Splicing* (Fig. 4). In the MIP, neuronal processes are easily distinguishable from background structures (Fig. 4a). Nevertheless, the tracing algorithm may generate a fragmented result (Fig. 4b,c), for example due to poorly stained regions in the axial direction. In such cases, the position label colors facilitate identification of potentially contiguous parts. However, the lack of depth information in a 2D projection view hampers user decision-making on which fragments are to be connected and in what order. By 3D rotation of the camera (Fig. 4d), human pattern recognition can quickly resolve this. Using the

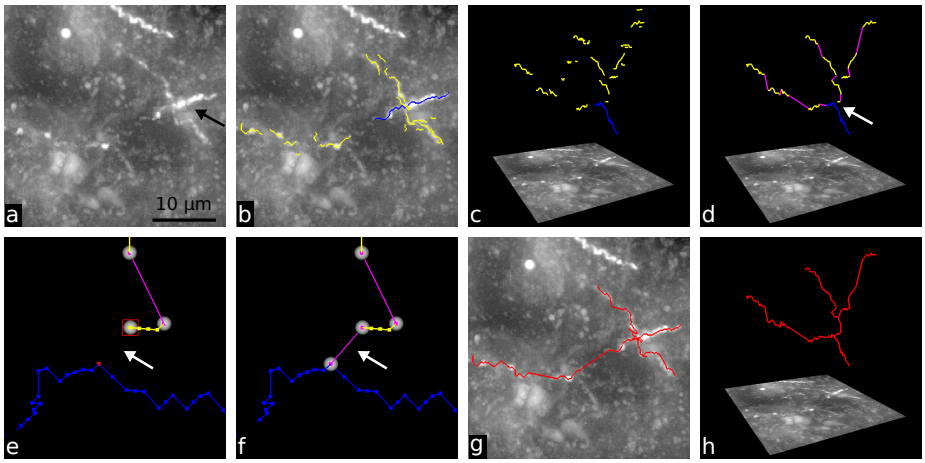

Figure 5: *Connecting edges at a branching point. (a) Axonal fragments (black arrow), whose 3D configuration is difficult to identify from the 2D MIP. (b) Even when displaying the position labels, the correct configuration remains ambiguous in 2D. (c) Rotation of the camera immediately reveals the three-dimensional configuration of the fragments. (d) After splicing axonal fragments (magenta segments) and removal of false segmentation results, branches may have to be connected at branching points (one such point is indicated by the arrow). (e) Close-up of the region pointed at by the arrow in (d). Nodes are displayed as circles, edge points as small squares. The edge point to be turned into a branching node and the terminal node of the upper edge are selected and (f) spliced, resulting in a point-to-node conversion and a new edge connecting the selected node with the new branching node. (g) The reconstruction result superimposed onto the MIP, and (h) viewed in 3D.*

selection and splicing tools of the FE, gaps between identified fragments can be closed (Fig. 4e–h).

Case 2: *Creating new branching points* (Fig. 5). A new branching connection is created by selecting a terminal node and a point on a different edge. The latter will be converted into a branching node (Fig. 5d,e) when applying the splice operation (Fig. 5f). The most likely location of the new branching node can easily be resolved by human pattern recognition, using the position-dependent coloring (Fig. 5b) and 3D camera rotation of the tracing and MIP (Fig. 5c). The *Splicing* operation invokes a *point-to-node* conversion of the selected point. The new node is connected to the selected node by a new edge, turning the former into a branching node. These steps result in a fully connected structure (Fig. 5g,h). Any intermediate nodes (having exactly two incident edges) are removed in a final step by invoking the *node-to-point* operation.

Case 3: Removal of false segmentations (Fig. 6). When all neurites in a particular region have been identified, falsely segmented fragments must be removed. In the present example, the *NeuroMorph* algorithms accept oversegmentation to ensure that no faintly stained axons are falsely discarded. The *Lasso* tool provides a dedicated mode (activated using a modifier key) to select only connected subgraphs that are entirely contained within a user-drawn polygon. This allows to select all small artifacts in the neighborhood of a re-

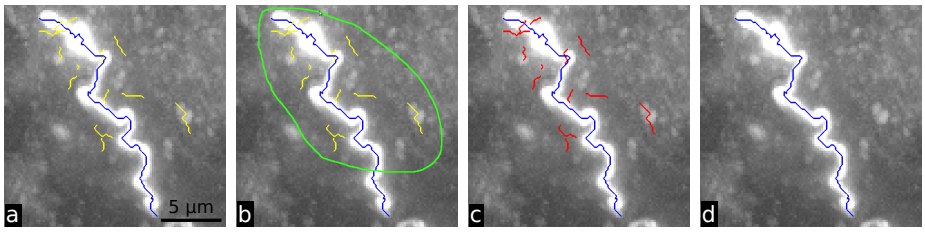

Figure 6: *Removal of false segmentations. (a) A correctly traced neurite segment (blue) is surrounded by oversegmented fragments (yellow). (b) To remove these, the lasso selection tool is employed, using the modifier key that ensures that only connected subgraphs are selected that are completely contained within the user-drawn polygon (green). (c) Thus only oversegmentations are selected (red), (d) which can be quickly deleted.*

constructed neuronal process at once and to delete them, without affecting the larger structure.

Case 4: *Removal of false connections* (Fig. 7). Occasionally, nearby branches may have been falsely connected by the tracing algorithm. Figure 7 illustrates how such situations are resolved. In the present example, the *NeuroMorph* algorithms created tracings whose spatial structure is difficult to verify from the 2D MIP image (Fig. 7a). The 3D view (Fig. 7b,c) reveals that the structure consists of two parallel axonal branches connected by a 'bridge'. Such bridges originate from limited resolution and are biologically implausible – they could result in loops in the neuronal tree – and must therefore be removed. To correct the false connection the user selects the bridging edge and removes it (Fig. 7d). After deletion of the edge, the defining nodes are no longer branching nodes. These intermediate nodes are removed using the node-to-point operation, joining its two incident edges (Fig. 7d).

3.1.3 Alignment and proof-editing across multiple image stacks

An important aspect of reconstructing complete 3D neuron morphologies is the merging of tracings obtained from multiple image stacks (e.g. consecutive brain sections). Here, tracings containing axonal branches from thalamocortical axons in eight consecutive brain sections were proof-edited as described above and then merged into a single *SpatialGraph* using the *CreateSpatialGraphStack module* (see Methods). The tracings obtained from each image stack were translated in the z-direction, i.e. perpendicular to the cutting plane, such that their bounding boxes adjoin.

The Align toolbox (Fig. 2a) in the FE was then used to rigidly align the subgraphs corresponding to each section tracing. The automated algorithm determined the correct transformation for all tracings in the 8-section data set. After alignment, the branches were connected across the section boundaries using the *Splicing* operation. The alignment and splicing process is regarded as the final quality control, as tracings of branches passing through multiple brain sections can be checked for continuity.

The final tracing result is scaled in the z-direction to match the vibratome-defined thickness of the brain sections (i.e. $8 \times 50\,\mu m = 400\,\mu m$), compensating

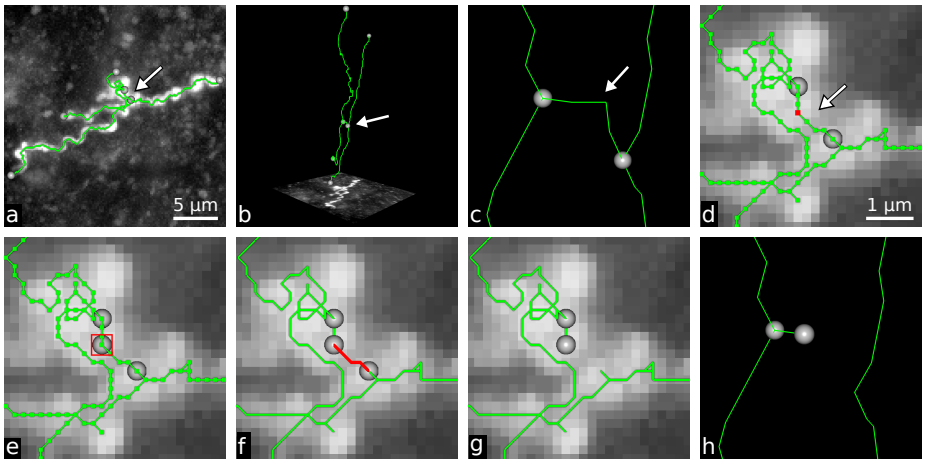

Figure 7: *Removal of false connections. (a) Axonal branches, superimposed on the MIP. Nodes are displayed as circles. The tracing is difficult to verify from this view. (b) The 3D view reveals that the tracing consists of two almost parallel axonal branches connected by a bridging edge (red) at the arrow, which is to be removed. (c) 3D close-up of the region around the false connection. (d) Resulting two separate branches (colored differently for visualization purposes) after deletion of the selected edge and node-to-point conversion of its defining nodes.*

for potential tissue shrinkage. Further, smoothing along the z-direction is applied (N=9, see Methods) to remove staircase artifacts in the skeletons due to anisotropic voxel sizes (i.e. $0.184\,\mu m$ in x/y, and $0.5\,\mu m$ in z). As a result, axonal branches of more than $1\,cm$ path length, including 31 branching points, were extracted from this example data set.

3.2 Inter-user variability of proof-editing *in vivo*-labeled neurons

The proof-editing of tracings obtained from individual image stacks, as well as the alignment and interconnection of tracings across image stacks, may introduce inter-user variability to the final 3D neuron reconstructions. Thus, we validate the above described tasks involving the FE by investigating the reproducibility of the final tracing result. To do so, five users proof-edited, merged and aligned the 8 tracings of the example data set. The users had varying degree of experience. One expert user has been involved in the development of the FE, two experienced users have been using the FE for approximately 12 months and two novice users only received a short introductory training.

Table 1 shows a comparison across users of the reconstruction results after proof-editing and merging (including smoothing and z-scaling) the 8 input tracings. As a first assessment of the inter-user variability, we compared the number of reconstructed axonal branches (i.e. edges in the *SpatialGraph*) and branch nodes. The results of the 5 users were essentially identical, given these coarse measures (i.e. 20 ± 0.84 branches, and 31 ± 0.71 branching nodes, mean±SD). Second, we investigated whether the extracted branches were similar in path

	U1	U2	U3	U4	U5	Mean	SD	% of mean
#Branches	20	19	20	21	19	20	0.84	4.2
#Branch points	31	31	31	32	30	31	0.71	2.3
Length (μm)	10762	10953	11053	11313	11153	11047	207	1.9
Time intra (min.)	344	209	118	130	405	241	129	53
Time inter (min.)	25	22	20	17	24	22	3.2	15

Table 1: *Comparison between 5 users (U1–U5) of the morphological properties of the final reconstructions. 'Branches' are edges in the SpatialGraph. 'Time intra' is the accumulated time in minutes required for proof-editing all eight input tracings. 'Time inter' is the time required for inter-section proof-editing, i.e., merging, alignment, interconnection, scaling, and z-smoothing. U1 and U5 are novice users, U2 and U3 are experienced users, U4 is an expert user.*

length. We find that the inter-user variability in path length is surprisingly small (SD=2% of the mean) for the present example data set of axonal branches from an *in vivo* labeled thalamocortical neuron.

While we could not observe any differences in tracing reliability across users, the time required for proof-editing deviated substantially with experience. Novice users (U1 and U5) need 2–3 times longer (344 and 405 minutes, respectively) than well-trained users (U2 and U3; 209 and 118 minutes, resp.). The difference between well-trained and the expert user (U4; 130 minutes) was less pronounced. In addition to the coarse comparison, we investigated the agreement between different users on branch trajectories (see Methods). The user agreement of a single example section (S01) and of the final result after alignment, interconnection, smoothing and z-scaling (S01–S08) is shown in Figure 8a,b and Figure 8c–f, respectively. To quantitatively describe the user agreement of the proof-edited tracings, we computed the accumulated length of all edge segments of each reconstruction that was agreed upon by the majority of the users (i.e. at least two other users found a corresponding segment). This length, expressed as a percentage of the total length, is computed for all users and for each of the eight tracings (Table 2).

	U1	U2	U3	U4	U5	Mean	SD
S01	95.6	96.1	97.0	96.5	87.5	94.5	3.5
S02	91.1	92.3	95.8	85.8	63.6	85.7	11.5
S03	95.6	94.3	96.4	98.7	64.6	89.9	12.7
S04	92.3	88.8	97.1	96.2	62.5	87.4	12.8
S05	88.5	96.8	96.9	95.5	85.5	92.6	4.7
S06	92.9	84.9	98.9	91.1	82.9	90.1	5.8
S07	96.7	92.6	96.4	94.3	88.2	93.7	3.1
S08	97.1	83.1	97.6	99.0	87.4	92.8	6.3
S01–08 (R=1 μm)	59.5	69.9	24.3	77.7	70.2	60.3	18.9
S01–08 (R=5 μm)	100.0	99.6	98.8	97.4	98.4	98.8	0.9

Table 2: *Fraction of length (%) found by three or more users for each section after intra-section proof-editing and the final reconstruction (S01–08) after inter-section splicing ($R = 0.5\,\mu m$, unless stated otherwise; $D = R/2$).*

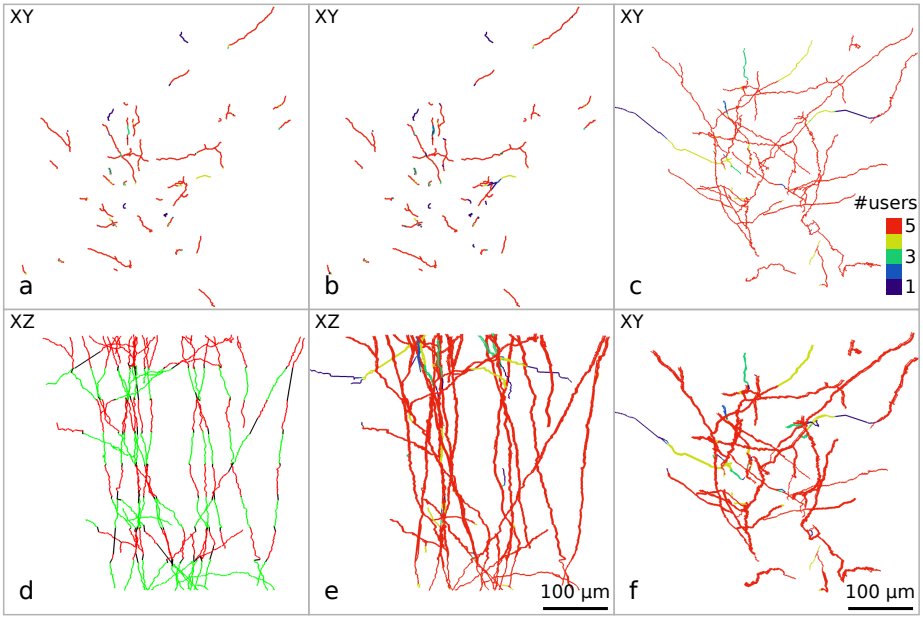

Figure 8: *User agreement between reconstructions. (a) Reconstruction of section S01 created by one of the users. Each edge point is colored by the number of users that found a corresponding point. (b) S01 reconstruction of all 5 users superimposed. (c) Reconstruction of all 8 sections by one of the users. (d) XZ-view of the reconstruction result of a single user showing the original sections (odd sections in green, even in red) and the interconnecting segments (black). (e) The results of all users superimposed (XZ-view). The bottom section remains untransformed, resulting in a virtually exact overlap between all users. Differences in alignment accumulate towards the top of the stack, resulting in minimally diverging branches. (f) XY-view on superimposed results of all users. Maximum sampling distance for single section (S01) comparison:* $D = 0.25\,\mu m$*; maximum correspondence distance:* $R = 0.5\,\mu m$ *(voxel length in z-direction). For comparison of entire stack:* $D = 2.5\,\mu m, R = 5\,\mu m$*.*

We find that, on average, between 85.7% and 94.5% of the tracings from individual image stacks are agreed upon by at least 3 users. The larger values of the standard deviation of particularly S02, S03 and S04 are mainly due to U5, whose proof-edited tracings have a relatively large fraction of branches not retained by the other users. These numbers have to be interpreted with caution. Inexperienced users (e.g. U5) may pursue a conservative approach, by retaining fragments that cannot doubtlessly be identified as foreground and by revisiting them during the inter-section proof-editing phase, where they can be judged within the context of the other brain sections. Consequently, retaining 'false positive' branches is not necessarily wrong, as long as they are removed during inter-section proof-editing.

Thus, we applied the same procedure for the completed reconstructions comprising the eight aligned and interconnected tracings (Table 2, S01–08). We find that for a small correspondence distance ($R = 1\,\mu m$) on average 60.3% of the total axon length is agreed upon by the majority of users. To investigate

whether this relatively small fraction is due to missing branches or differences in alignment, the correspondence distance was increased to $5\,\mu m$, resulting in an average agreement of 98.8%. Thus, virtually all branches had counterparts and the large fraction of unmatched braches (i.e. at $R = 1\,\mu m$ resolution) must originate from small differences in alignment, as illustrated in Figure 8.

In a previous study (Dercksen et al., 2009) we showed that the automated alignment method yields results comparable to those produced by an expert user when aligning the same data sets. However, in the present example, we compare the alignment between data sets that are slightly different due to inter-user differences after proof-editing tracings of each image stack. All sections in all five data sets could be successfully aligned using the default parameters (distance threshold $d = 10\,\mu m$ and weighting factor $\alpha = 0.25$, see (Dercksen et al., 2009)). Differences in rotation and translation between users are listed in Table 3. We find that these differences are small. Rotations differ by at most 0.33 degree, translations by at most $4.04\,\mu m$ and $4.17\,\mu m$ in x and y, respectively.

	$R(^\circ)$		$T_x(\mu m)$		$T_y(\mu m)$	
	max-min	SD	max-min	SD	max-min	SD
S02	0.11	0.04	1.66	0.58	2.14	0.71
S03	0.03	0.01	0.44	0.18	0.17	0.06
S04	0.25	0.09	2.49	0.81	3.85	1.27
S05	0.33	0.13	3.94	1.52	4.17	1.57
S06	0.13	0.05	1.56	0.60	1.44	0.54
S07	0.27	0.09	1.36	0.43	3.68	1.32
S08	0.13	0.05	4.04	1.44	3.46	1.22

Table 3: *Inter-user differences in alignment. Each row lists the difference between maximum and minimum rotation angle (R), translation in x- and y-direction (T_x, T_y) of each section with respect to its preceding section (S01 remains untransformed), as well as the standard deviation (SD) of all 5 users.*

In summary, comparison of the proof-editing results produced by five different users indicates a high degree of accuracy of the final morphology. First, coarse comparison yielded only small differences in the number of branches (∼1 error per 20 branches), branching nodes (∼1 error per 31 branching nodes) and total length (∼$19\,\mu m$ error per $1\,mm$ axon, see Table 1). Second, agreement in trajectories after proof-editing varied between 85.7% and 94.5% across individual image stacks (Table 2). Third, differences in alignment are small, i.e. ∼$4\,\mu m$ (Table 3). Consequently, the trajectories of the final reconstructions across multiple image stacks are very similar: on average 98.8% of the reconstructed trajectories were identical across users, using a correspondence radius of $5\,\mu m$. No significant differences were measured between expert and novice users. Specifically, the consensus length was computed for two groups consisting of the three most (U2, U3, U4) and three least experienced (U1, U3, U5) users, respectively. The average consensus length (i.e., at least 2 of 3 users agreed) as a percentage of the total length was 98.7% for the less experienced and 98.8% for the more experienced group (using the correspondence distance of $R = 5\,\mu m$). However, the amount of manual labor required for proof-editing automated tracings decreases with experience from ∼6.5 to ∼2 hours per cen-

timeter axon.

4 Discussion

4.1 Applicability and inter-user variability of the Filament Editor

The FE combines various visualization, selection and operation functionalities that allow interactive proof-editing and analysis of 3D neuronal tracings within an easy-to-use and intuitive GUI. Using an example dataset of *in vivo* labeled thalamocortical axons from eight consecutive large, high-resolution image stacks, we illustrated four general situations that may occur during proof-editing any sparsely labeled morphology data. The relative abundance of each of the four use cases will however strongly depend on the image and labeling quality, as well as on the accuracy of the automated or manual tracing methods.

The example data set used here, can be regarded as one of the most challenging cases for reconstructing complete and accurate 3D neuron morphologies. First, the neurons were labeled in rat thalamus *in vivo*, whereas its axonal branches were imaged within vibrissal cortex, about $3\,mm$ away from the recording site. Thus, in addition to faint staining caused by thin axonal diameters, diffusion of the tracer (i.e., biocytin) along centimeters of axon may have further decreased signal-to-noise ratios of terminal branches. Second, due to the large axonal innervation volume, here $2\,mm \times 2\,mm \times 1\,mm$, the tissue was imaged using a brightfield microscope (at a resolution at the diffraction limit of light) at the cost of contrast and axial resolution. Any fluorescent microscope system of superior contrast and resolution (e.g. 2-photon) would require impractically long imaging times, compared to the ∼24 hours required using the present system (Oberlaender, Broser, et al., 2009; Oberlaender, Bruno, et al., 2007).

Finally, because of the faint labeling and limited contrast, the automated tracing algorithms (i.e. as implemented within the *NeuroMorph* pipeline) accept oversegmentation to guarantee that all axonal fragments are reconstructed, at the cost of picking up also background structures. The completeness of detecting and tracing all axonal fragments by the *NeuroMorph* system has been validated against manual results generated by human expert users previously (Oberlaender, Bruno, et al., 2007). Consequently, because the FE allows unambiguous proof-editing of the thalamocortical axons presented, datasets of higher contrast, higher resolution or less background will certainly allow for an even faster and equally reliable proof-editing of complete 3D morphologies using the FE.

Using a challenging dataset, we illustrated that the combination of 3D image data (e.g. as a 2D MIP) with (i) 3D tracings (edges are rendered as polylines, nodes as spheres, points as squares), (ii) semantic labeling, (iii) 3D viewing (i.e. camera rotation, translation and zoom), as well as (iv) 3D selecting, hiding and editing is a convenient, intuitive and fast approach to extract reliable 3D morphologies from large sparsely labeled images. Here, about 0.5 terabyte of image data, containing more than one centimeter of axonal fragments could be proof-edited with 98.8% accuracy within 2–6 hours, the proof-editing time depending on the experience of the operator.

4.2 Comparison to other proof-editing tools

Peng et al. (Peng, Long, et al., 2011) argue that despite great advances in automated tracing methods (see (Donohue and Ascoli, 2011; Meijering, 2010) for reviews), proof-editing remains a necessary, but laborious process. Besides a fully automated proof-editing system that learns by example to predict the different error types and their bounds, Peng et al. regard a highly ergonomic 3D interactive WYSIWIG (What You See Is What You Get) system as a solution to this problem. Although a wide array of digital tracing tools are available (the most used one, *Neurolucida* (www.mbfbioscience.com), as well as a variety of alternative tools are reviewed in (Meijering, 2010; Parekh and Ascoli, 2013)), only few software packages implement a system that provides effective visual verification and fast interactive correction of tracings. The *FARSIGHT Trace Editor* (Luisi et al., 2011), *V3D* (Peng, Ruan, et al., 2010), *Neuromantic* (Myatt et al., 2012), *NeuronStudio* (Wearne et al., 2005) and *SpineLab* (Jungblut et al., 2012) are examples of tools that provide simultaneous display of image and tracing data for verification and a set of tools to modify the latter. Some aspects in which the above mentioned tools differ are the degree of usability (e.g. undo/redo functionality), whether the tracing can be viewed and edited in 3D, the available measurement functions and supported platforms (Windows, Linux, Mac).

The FE was designed and implemented to meet high standards with respect to all of these aspects. Further, and in contrast to the above mentioned tools, the FE has been designed to meet the specific demands of *in vivo* labeled datasets. The general challenges for validating neuronal tracings from *in vivo* data arise from the (i) the large innervation volumes of individual axons (e.g., $\sim 12\,mm^3$ for L5 slender-tufted pyramidal neurons (L5st, see Figure 3b) in rat vibrissal cortex (S1) (Oberlaender, Boudewijns, et al., 2011)), (ii) the complexity of the axonal arbor (e.g., $86.8 \pm 5.5\,mm$ path length, 216 ± 35 bifurcation points for L5st in S1) and (iii) axonal diameters as thin as $100\,nm$. Consequently, validating *in vivo* tracings can be considered as at least one order of magnitude more complex (i.e., in terms of imaging volume, axonal path length and topology) compared to *in vitro* data from the same species, brain region and cell type (e.g., L5st axon length in S1 from *in vitro* tracings was reported as $7.8 \pm 2.5\,mm$ (Frick et al., 2008)). These challenges are for example illustrated by the fact that, at present, the NeuroMorpho.org repository comprises 5,405 neocortical neurons from various species, but only 3% (188 neurons) of them were labeled *in vivo* and only 0.4% (21 neurons) contain both, reconstructed dendrites and axons. Moreover, none of these 21 neurons were reconstructed at a magnification of $100\times$ (i.e., as was the present example dataset), which may be critical to reliably detect all axonal projections (Oberlaender, Broser, et al., 2009).

The Filament Editor provides proof-editing strategies to overcome the challenges described above. First, we incorporated 3D visualization and 3D editing routines that remain functional for imaging volumes and tracing complexities beyond typical *in vitro* datasets. For example (i) the data structure was designed to render and edit large filament data sets, a consequence of the complexity of *in vivo* labeled morphologies and of oversegmented automated tracings results, while maintaining interactive usability. (ii) The selection system allows the user to efficiently highlight the desired part of the tracing based on location (single click, lasso selection), connectivity (connected component), or semantic label

for editing or visualization. (iii) Selectively hiding parts of the tracing allows focusing on specific regions of large structures without visual clutter. (iv) As shown in the results, the semantic labeling feature enables position-dependent labels, which visually support user decision making on what neuronal fragments are to be connected or discarded. Second, we integrated alignment and splicing functionalities to merge multi-section datasets, allowing for a final quality control by checking continuity of tracings across brain sections. Again, the semantic labeling eases across-section editing by visualizing edges from different sections in different colors.

Other unique features of the Filament Editor include simultaneous display and quantitative comparison of tracings for assessing inter-user variability, as well as morphometric analysis with respect to 3D anatomical structures. Taken together, the FE will help increasing the so far negligible number of validated 3D neuron tracings from *in vivo* preparations.

5 Conclusion

We presented the Filament Editor (FE), a software toolbox integrating components for proof-editing neuron tracings in 3D, across-section alignment and morphometric analysis. The effectiveness of the FE was demonstrated on the example of *in vivo* labeled axonal branches from multiple brightfield image stacks. The FE addresses a clear need for efficient and effective proof-editing, advancing the possibilities for high-throughput reconstruction of accurate and complete 3D neuron morphology. Altogether, the FE facilitates quantitative neuroanatomical studies from *in vivo* labeled data, as previously illustrated on the examples of determining cell types (Oberlaender, Kock, et al., 2012), axon projection patterns (Oberlaender, Boudewijns, et al., 2011), plasticity during sensory deprivation (Oberlaender, Ramirez, et al., 2012) or simulations of sensory-evoked signal flow (Lang et al., 2011).

Information Sharing Statement

The Filament Editor and the associated modules described in this article can be obtained by acquiring Amira 5.5 and installing the ZIB extension package as described on following website:
`www.zib.de/en/visual/software/neuronreconstruction.html`
Data used to generate images and results can also be downloaded. The authors declare that they have no conflict of interest.

Acknowledgments

We thank Bert Sakmann and Philip J. Broser for advice and assistance during early stages of the project; Wolfgang Holler and Britta Weber for their contribution to the Filament Editor; Marianne Krabi and Jonas Hörsch for assisting with the analysis functionality; Norbert Lindow for providing the LineRayCaster. Randy M. Bruno and Christiaan P.J. de Kock for supplying biocytin-labeled neurons; Lothar Baltruschat, Richard Smith, Kevin Pels, and Ariel Lee for

proof-editing; Hans-Joachim Wagner and the entire staff of the Anatomy Institute of the University of Tuebingen for their generous support. Funding was provided by the Bernstein Center for Computational Neuroscience, Tuebingen (funded by the German Federal Ministry of Education and Research (BMBF; FKZ: 01GQ1002)) (MO), by the Max Planck Institute for Biological Cybernetics, Tuebingen (MO), by the Max Planck Florida Institute for Neuroscience, Jupiter (MO), by the Werner Reichardt Center for Integrative Neuroscience, Tuebingen (MO), by the Zuse Institute Berlin (VJD, HCH) and the Max Planck Institute of Neurobiology, Martinsried (VJD). The funders had no role in study design, data collection and analysis, decision to publish, or preparation of the manuscript.

Author Contributions

Conceived and designed the project: MO. Developed the Filament Editor and associated functionalities: VJD. Analyzed the data and wrote the paper: VJD, HCH, MO.

References

Ascoli, GA (2006). "Mobilizing the base of neuroscience data: the case of neuronal morphologies." *Nature Reviews Neuroscience*, 7(4), pp. 318–324.

Ascoli, GA, DE Donohue, and M Halavi (2007). "NeuroMorpho.Org: a central resource for neuronal morphologies." *The Journal of Neuroscience*, 27(35), pp. 9247–9251.

Binzegger, T, RJ Douglas, and KAC Martin (2004). "A quantitative map of the circuit of cat primary visual cortex." *The Journal of Neuroscience*, 24(39), pp. 8441–8453.

Broser, PJ, V Grinevich, P Osten, B Sakmann, and DJ Wallace (2008). "Critical Period Plasticity of Axonal Arbors of Layer 2/3 Pyramidal Neurons in Rat Somatosensory Cortex: Layer-Specific Reduction of Projections into Deprived Cortical Columns". *Cerebral Cortex*, 18(7), pp. 1588–1603.

Broser, PJ, R Schulte, S Lang, A Roth, F Helmchen, J Waters, B Sakmann, and G Wittum (2004). "Nonlinear anisotropic diffusion filtering of three-dimensional image data from two-photon microscopy." *Journal of Biomedical Optics*, 9(6), pp. 1253–64.

Cannon, RC, DA Turner, GK Pyapali, and HV Wheal (1998). "An on-line archive of reconstructed hippocampal neurons." *Journal of Neuroscience Methods*, 84(1-2), pp. 49–54.

Carnevale, NT and ML Hines (2006). *The NEURON Book*. Cambridge University Press.

Crook, S, P Gleeson, F Howell, J Svitak, and RA Silver (2007). "MorphML: Level 1 of the NeuroML Standards for Neuronal Morphology Data and Model Specification". *Neuroinformatics*, 5(2), pp. 96–104.

Dercksen, VJ, B Weber, D Günther, M Oberlaender, S Prohaska, and HC Hege (2009). "Automatic alignment of stacks of filament data". In: *Proc. IEEE International Symposium on Biomedical Imaging: From Nano to Macro, Boston, USA*, pp. 971–974.

Dodt, HU, U Leischner, A Schierloh, N Jährling, CP Mauch, K Deininger, JM Deussing, M Eder, W Zieglgänsberger, and K Becker (2007). "Ultramicroscopy: three-dimensional visualization of neuronal networks in the whole mouse brain". *Nature Methods*, 4(4), pp. 331–336.

Donohue, DE and GA Ascoli (2011). "Automated reconstruction of neuronal morphology: an overview." *Brain Research Reviews*, 67(1-2), pp. 94–102.

Ertürk, A, CP Mauch, F Hellal, F Förstner, T Keck, K Becker, N Jährling, H Steffens, M Richter, M Hübener, E Kramer, F Kirchhoff, HU Dodt, and F Bradke (2012). "Three-dimensional imaging of the unsectioned adult spinal cord to assess axon regeneration and glial responses after injury." *Nature Medicine*, 18(1), pp. 166–71.

FEI-Visualization Sciences Group (2013a). *Amira 5.5*.

— (2013b). *Amira 5.5 Reference Guide*.

Feldmeyer, D and B Sakmann (2000). "Synaptic efficacy and reliability of excitatory connections between the principal neurones of the input (layer 4) and output layer (layer 5) of the neocortex". *The Journal of Physiology*, 525(Pt 1), pp. 31–39.

Frick, A, D Feldmeyer, M Helmstaedter, and B Sakmann (2008). "Monosynaptic connections between pairs of L5A pyramidal neurons in columns of juvenile rat somatosensory cortex." *Cerebral Cortex*, 18(2), pp. 397–406.

Fuchs, H, ZM Kedem, and SP Uselton (1977). "Optimal Surface Reconstruction from Planar Contours". *Communications of the ACM*, 20(10), pp. 693–702.

Gillette, Ta, KM Brown, and Ga Ascoli (2011). "The DIADEM metric: comparing multiple reconstructions of the same neuron." *Neuroinformatics*, 9(2-3), pp. 233–245.

Groh, A, HS Meyer, EF Schmidt, N Heintz, B Sakmann, and P Krieger (2010). "Cell-type specific properties of pyramidal neurons in neocortex underlying a layout that is modifiable depending on the cortical area." *Cerebral Cortex*, 20(4), pp. 826–836.

Halavi, M, Ka Hamilton, R Parekh, and Ga Ascoli (2012). "Digital reconstructions of neuronal morphology: three decades of research trends." *Frontiers in Neuroscience*, 6(49).

Helmstaedter, M, KL Briggman, and W Denk (2011). "High-accuracy neurite reconstruction for high-throughput neuroanatomy." *Nature Neuroscience*, 14(8), pp. 1081–1088.

Hill, SL, Y Wang, I Riachi, F Schürmann, and H Markram (2012). "Statistical connectivity provides a sufficient foundation for specific functional connectivity in neocortical neural microcircuits." *Proceedings of the National Academy of Sciences of the United States of America*, 109(42), E2885–94.

Horikawa, K and WE Armstrong (1988). "A versatile means of intracellular labeling: injection of biocytin and its detection with avidin conjugates." *Journal of Neuroscience Methods*, 25(1), pp. 1–11.

Jungblut, D, A Vlachos, G Schuldt, N Zahn, T Deller, and G Wittum (2012). "SpineLab: tool for three-dimensional reconstruction of neuronal cell morphology". *Journal of Biomedical Optics*, 17(7), p. 076007.

Kleinfeld, D, A Bharioke, P Blinder, DD Bock, KL Briggman, DB Chklovskii, W Denk, M Helmstaedter, JP Kaufhold, WCA Lee, HS Meyer, KD Micheva, M Oberlaender, S Prohaska, RC Reid, SJ Smith, S Takemura, PS Tsai, and B Sakmann (2011). "Large-scale automated histology in the pursuit of connectomes." *The Journal of Neuroscience*, 31(45), pp. 16125–16138.

Lang, S, VJ Dercksen, B Sakmann, and M Oberlaender (2011). "Simulation of Signal Flow in Three-Dimensional Reconstructions of an Anatomically Realistic Neuronal Network in Rat Vibrissal Cortex". *Neural Networks*, 24(9), pp. 998–1011.

Liang, YD, BA Barsky, and M Slater (1992). *Some Improvements to a Parametric Line Clipping Algorithm*. Tech. rep. UCB/CSD-92-688. EECS Department, University of California, Berkeley.

Luisi, J, A Narayanaswamy, Z Galbreath, and B Roysam (2011). "The FARSIGHT Trace Editor: An Open Source Tool for 3-D Inspection and Efficient Pattern Analysis Aided Editing of Automated Neuronal Reconstructions." *Neuroinformatics*, 9(2-3), pp. 305–315.

Margrie, TW, M Brecht, and B Sakmann (2002). "In vivo, low-resistance, whole-cell recordings from neurons in the anaesthetized and awake mammalian brain". *Pflügers Archiv : European Journal of Physiology*, 444(4), pp. 491–498.

Markram, H (2006). "The Blue Brain Project". *Nature Reviews Neuroscience*, 7(2), pp. 153–160.

Mayerich, D, C Bjornsson, J Taylor, and B Roysam (2011). "Metrics for Comparing Explicit Representations of Interconnected Biological Networks". In: *IEEE Symposium on Biological Data Visualization*, pp. 79–86.

McGuffin, MJ and I Jurisica (2009). "Interaction techniques for selecting and manipulating subgraphs in network visualizations." *IEEE Transactions on Visualization and Computer Graphics*, 15(6), pp. 937–944.

Meijering, E (2010). "Neuron tracing in perspective." *Cytometry Part A*, 77(7), pp. 693–704.

Meyer, HS, VC Wimmer, M Hemberger, RM Bruno, CPJ De Kock, A Frick, B Sakmann, and M Helmstaedter (2010). "Cell Type-Specific Thalamic Innervation in a Column of Rat Vibrissal Cortex". *Cerebral Cortex*, 20(10), pp. 2287–2303.

Myatt, DR, T Hadlington, GA Ascoli, and SJ Nasuto (2012). "Neuromantic – from semi-manual to semi-automatic reconstruction of neuron morphology". *Frontiers in Neuroinformatics*, 6(4).

Nielsen, J and RL Mack (1994). *Usability inspection methods*. New York: John Wiley & Sons, Inc.

Oberlaender, M, ZSRM Boudewijns, T Kleele, HD Mansvelder, B Sakmann, and CPJ De Kock (2011). "Three-dimensional axon morphologies of individual layer 5 neurons indicate cell type-specific intracortical pathways for whisker motion and touch". *Proceedings of the National Academy of Sciences*, 108(10), pp. 4188–4193.

Oberlaender, M, PJ Broser, B Sakmann, and S Hippler (2009). "Shack-Hartmann wave front measurements in cortical tissue for deconvolution of large three-dimensional mosaic transmitted light brightfield micrographs". *Journal of Microscopy*, 233(2), pp. 275–289.

Oberlaender, M, RM Bruno, B Sakmann, and PJ Broser (2007). "Transmitted light brightfield mosaic microscopy for three-dimensional tracing of single neuron morphology". *Journal of Biomedical Optics*, 12(6), pp. 1–19.

Oberlaender, M, CPJ de Kock, RM Bruno, A Ramirez, HS Meyer, VJ Dercksen, M Helmstaedter, and B Sakmann (2012). "Cell Type-Specific Three-Dimensional Structure of Thalamocortical Circuits in a Column of Rat Vibrissal Cortex". *Cerebral Cortex*, 22(10), pp. 2375–2391.

Oberlaender, M, A Ramirez, and RM Bruno (2012). "Sensory Experience Restructures Thalamocortical Axons during Adulthood". *Neuron*, 74(4), pp. 648–655.

Parekh, R and GA Ascoli (2013). "Neuronal Morphology Goes Digital: A Research Hub for Cellular and System Neuroscience". *Neuron*, 77(6), pp. 1017–1038.

Peng, H, F Long, T Zhao, and E Myers (2011). "Proof-editing is the bottleneck of 3D neuron reconstruction: the problem and solutions." *Neuroinformatics*, 9(2-3), pp. 103–105.

Peng, H, Z Ruan, F Long, JH Simpson, and EW Myers (2010). "V3D enables real-time 3D visualization and quantitative analysis of large-scale biological image data sets." *Nature Biotechnology*, 28(4), pp. 348–353.

Pinault, D (1996). "A novel single-cell staining procedure performed in vivo under electrophysiological control: morpho-functional features of juxtacellularly labeled thalamic cells and other central neurons with biocytin or Neurobiotin." *Journal of Neuroscience Methods*, 65(2), pp. 113–136.

Ragan, T, LR Kadiri, KU Venkataraju, K Bahlmann, J Sutin, J Taranda, I Arganda-Carreras, Y Kim, HS Seung, and P Osten (2012). "Serial two-photon tomography for automated ex vivo mouse brain imaging." *Nature Methods*, 9(3), pp. 255–258.

Schubert, D, R Kötter, HJ Luhmann, and JF Staiger (2006). "Morphology, electrophysiology and functional input connectivity of pyramidal neurons characterizes a genuine layer Va in the primary somatosensory cortex." *Cerebral Cortex*, 16(2), pp. 223–236.

Sigg, C, T Weyrich, M Botsch, and M Gross (2006). "GPU-based ray-casting of quadratic surfaces". In: *Proceedings IEEE/Eurographics Symposium on Point-Based Graphics*. Boston, MA, pp. 59–65.

Skiena, SS (1998). *The algorithm design manual*. Springer Verlag New York, Inc.

Svoboda, K (Sept. 2011). "The past, present, and future of single neuron reconstruction." *Neuroinformatics*, 9(2-3), pp. 97–98.

Szeliski, R (2006). "Image Alignment and Stitching: A Tutorial". *Foundations and Trends in Computer Graphics and Vision*, 2(1), pp. 1–104.

Wearne, SL, A Rodriguez, DB Ehlenberger, AB Rocher, SC Henderson, and PR Hof (2005). "New Techniques for Imaging, Digitization and Analysis of Three-Dimensional Neural Morphology on Multiple Scales". *Neuroscience*, 136, pp. 661–680.

Wills, G (1996). "524,288 Ways to Say "This is Interesting"". In: *Proceedings IEEE Symposium on Information Visualization*. San Francisco, CA, pp. 54–61.

Wong-Riley, M (1979). "Changes in the visual system of monocularly sutured or enucleated cats demonstrable with cytochrome oxidase histochemistry". *Brain research*, 171(2), pp. 11–28.

Zitová, B and J Flusser (2003). "Image registration methods: a survey". *Image and Vision Computing*, 21(11), pp. 977–1000.